Food Packaging and Shelf Life 42 (2024) 101244

Contents lists available at ScienceDirect

Food Packaging and Shelf Life

journal homepage: www.elsevier.com/locate/fpsl

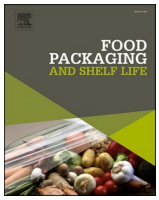

Biodegradable and recyclable bio-based laminated films of poly (lactic acid) and cellulose nanocrystals for food barrier packaging

Cong Chen [a,b], Lu Wang [c], Siamak Shams Es-haghi [b,d], Mehdi Tajvidi [a,b], Jinwu Wang [a,b,e,*,1], Douglas J. Gardner [a,b,**,2]

[a] School of Forest Resources, University of Maine, Orono, ME 04469, United States
[b] Advanced Structures and Composites Center, University of Maine, Orono, ME 04469, United States
[c] Center for Renewable Carbon & School of Natural Resources, The University of Tennessee, Knoxville, TN 37996, United States
[d] Department of Chemical and Biomedical Engineering, University of Maine, Orono, ME 04469, United States
[e] Forest Products Laboratory, US Forest Service, 1 Gifford Pinchot Drive, Madison, WI 53726, United States

ARTICLE INFO

Keywords:
Food packaging
Polylactic acid
Cellulose nanocrystals
Barrier properties
Laminated film

ABSTRACT

Exploring food packaging films from environmentally friendly materials and their practical manufacturing routes are important research topics for academia and industry. Poly (lactic acid) (PLA) is a bio-based plastic being used commercially but with low barrier performance for food packaging applications. Cellulose nanocrystals (CNCs), as renewable materials, show potential use in packaging applications, attributed to their excellent oxygen barrier performance. However, pure CNC films cannot be readily produced and used because of their brittleness and water sensitivity. Creating a multilayer structure may be a promising way to address the issues associated with PLA or CNCs if applied as a single-component packaging material. In this work, CNC suspensions mixed with 15 wt% polyvinyl alcohol (PVA) or kappa-carrageenan (CG) were directly coated on a PLA substrate, followed by lamination without any petroleum-based tie layer or adhesive addition. These three-layer laminate films exhibited enhanced barrier properties. The oxygen permeability of the multilayer film was more than 70 times lower than pure PLA film, and the water vapor permeability decreased 7-fold compared with the pure CNC film. Moreover, the PLA film protects the inner CNC film from water and mechanical damage. In addition, the PLA film could be easily separated and recycled from the multilayer film by soaking it in water after the end of use. The fabricated multilayer PLA-CNC films are ideal for eco-friendly, recyclable, high-performance food packaging applications.

1. Introduction

Packaging protects food from external influences and damage, maintains food safety, and extends shelf life in a cost-effective way (Coles, Mcdowell, & Kirwan, 2003; Marsh & Bugusu, 2007). Among the variety of packaging materials, plastics occupy a large proportion of the commercial market (Piergiovanni & Limbo, 2016), owing to their attractive properties, such as high strength, excellent barrier performance, flexibility, lightweight, good processability, and low cost (Narancic & O'connor, 2018; Qasim et al., 2021; Sangroniz et al., 2019). However, conventional plastics are derived from petroleum resources. Coupled with single-use culture, packaging applications of petroleum-based plastics are causing serious environmental pollution and the loss of resources (Haward, 2018; Narancic & O'connor, 2018). Driven by environmental and fossil resources saving awareness, renewable, biodegradable, and recyclable bio-based polymers are attracting enormous attention from the scientific, industrial, as well as consumer perspective (Helanto et al., 2019; Kawashima et al., 2019; Reddy et al., 2013; Wang, Gardner, et al., 2020).

Among the diverse variety of bio-based polymers, poly (lactic acid)

* Correspondence to: Forest Products Laboratory, U.S. Forest Service, Madison, Wisconsin 53726, United States.
** Correspondence to: Advanced Structures and Composites Center, University of Maine, Orono, Maine 04469-5793, United States; School of Forest Resources, University of Maine, Orono, Maine 04469-5755, United States.
E-mail addresses: jinwu.wang@usda.gov (J. Wang), douglasg@maine.edu (D.J. Gardner).
[1] orcid.org/0000-0002-8363-1689
[2] orcid.org/0000-0002-2903-2570

https://doi.org/10.1016/j.fpsl.2024.101244
Received 2 October 2023; Received in revised form 8 December 2023; Accepted 21 January 2024
Available online 2 February 2024

(PLA) and cellulose have been proposed as promising alternatives to potentially address the demand for renewable materials for food packaging (Cazón et al., 2017; Helanto et al., 2019; Jamshidian et al., 2010). Lactic acid (or lactide), the monomer of PLA, is manufactured by carbohydrate fermentation or chemical synthesis from 100% plant sources, including corn and rice starch, and sugar cane among other raw materials (Auras et al., 2004; Jariyasakoolroj et al., 2020; Muller et al., 2017). On the other hand, cellulose stands out as the most abundant renewable natural polymer on earth (Habibi, Lucia, & Rojas, 2010; Kargarzadeh et al., 2017). As a bio-based plastic, PLA has been commercially used in food packaging applications attributed to its high mechanical properties, thermal plasticity, and biocompatibility (Ahmed & Varshney, 2011), making it suitable for a broad array of products, especially in short shelf-life and fresh products (Auras et al., 2004; Auras et al., 2003). For food packaging applications, besides environmental awareness, barrier properties are an essential attribute in modern packaging to reduce food deterioration. However, the oxygen barrier performance of a neat PLA film is insufficient for certain food packaging requirements. This limitation could be improved by cellulose nanocrystals (CNCs), one major type of cellulose nanomaterials (CNMs), known for their extraordinary oxygen barrier performance under dry conditions (Dhar et al., 2014; Mu et al., 2019). CNCs are extracted from renewable biomass resources by acid hydrolysis with amorphous regions removed and crystalline regions remaining, which leads to a high degree of crystallinity (Trache et al., 2017). The high crystallinity of CNC films impedes gas permeation to enhance the oxygen barrier performance (Chowdhury, Nuruddin, et al., 2018). Within the prepared dried films, CNC particles arrange in an ordered layered structure and form high-density strong hydrogen bonding, which leads to tortuous gas diffusion paths. Meanwhile, the difference in polarity between oxygen and CNCs also results in a low oxygen solubility of films (Wang et al., 2020). These features endow CNC films with an extraordinary oxygen barrier performance. Moreover, the high visible light transparency and mechanical strength of CNC films are additional advantages for food packaging applications (Ahankari et al., 2021; Hubbe et al., 2017; Stark, 2016). Nevertheless, the drawbacks of brittleness and water sensitivity of neat CNC films hinder their use in several food packaging applications. Consequently, the combination of PLA and CNCs may provide a promising way to overcome the downside of either mono-material for developing sustainable food packaging (Gan & Chow, 2018). Previous studies have shown that incorporating CNCs into PLA can enhance the barrier properties of fabricated biocomposite films. (Dhar et al., 2017; Fortunati et al., 2012; Karkhanis et al., 2018; Liu & Matuana, 2019; Sung et al., 2017). Although PLA is a biocompatible polymer, chemical modifications, organic solvents, or complicated processing steps were necessary when blending CNCs with PLA (Dhar et al., 2016; Fortunati et al., 2012; Gazzotti et al., 2017). On the other hand, conventional extrusion methods enable the introduction of CNCs into PLA matrices without using solvents or modifications. However, CNCs often need to be freeze-dried into a powder when combined with PLA pellets during extrusion. This powder form tends to cause CNCs agglomeration within the prepared films (Karkhanis et al., 2018; Liu & Matuana, 2019; Sung et al., 2017). Furthermore, a continuous barrier layer is difficult to be obtained attributable to the low CNCs content ($\leq$ 5 wt%) in the composite film. Despite all the efforts, the extraordinary oxygen barrier capability of CNCs cannot be preserved completely in the composite films.

Multilayer films with CNM films in the core and plastic films as protective skins have been demonstrated as a feasible technology by food packaging researchers. In this multilayer structure, CNM films play a key function in the oxygen barrier property. Meanwhile, plastic layers can retard moisture permeation and prevent CNM films from being degraded by ambient mechanical or chemical attacks (Wang et al., 2018). The water vapor and oxygen transmission rate of multilayer films were significantly decreased by laminating plastic films together with CNM films using an adhesive tie layer (Du et al., 2021; Fotie et al., 2020; Wang, Chen, et al., 2020). The oxygen barrier of multilayer PLA films was enhanced by neat or rosin-modified CNM films as an inner layer followed by 170 °C hot pressing (Le Gars et al., 2020). These findings collectively confirm that lamination is an effective strategy for manufacturing bio-based barrier films for food packaging applications.

However, the high viscosity and difficulty of coating CNC suspensions on low surface energy polymers affect the processability of CNCs. The addition of carboxymethyl cellulose (CMC) was reported to provide a substantially homogeneous composition of CNC suspensions and the resulting films (Youngblood et al., 2022). It is generally believed that the addition of soluble polymers can modify the viscosity and surface tension of an aqueous suspension that contributes to coating uniformity and thickness. Generally, there are three kinds of water-soluble polymers used for changing the behavior of CNC suspensions: cationic polymers such as chitosan, anionic polymers such as CMC and kappa-carrageenan (CG), and nonionic polymers such as polyvinyl alcohol (PVA). Because the surface of CNC particles is negatively charged attributable to sulfate ester groups, anionic polymers would be less likely to interact with CNCs but can induce depletion flocculation of the system, which induces the particles to come closer to each other. Cationic polymers can be adsorbed on negatively charged CNC surfaces to bridge particles. Generally, the thinning effect of various polymers on CNC suspensions was found to have the following trend: nonionic > anionic > cationic (Peng et al., 2018). In addition to charge changes, the degree of modification to CNC suspensions can be influenced by molecular structure, weight, and conformation. PVA was found to improve the physical properties of the resulting PVA/CNC coating (Huang et al., 2022), while decreasing the viscosity of CNC suspensions at intermediate shear rates (Nuruddin et al., 2021) which may have a positive impact on handling, e.g., pumping/transportation, and/or subsequent applications such as coating.

In this study, tri-layer PLA-CNC-PLA films without a tie layer or CNC modification were successfully prepared for sustainable food packaging by coating and lamination. In this tri-layer structure combining both advantages of PLA and CNCs, CNCs were designed as the core layer for oxygen barrier purpose, and the two outer PLA layers provide necessary protection against water and physical damage. To overcome the compatibility issue between PLA and CNC films and improve the processability, a nonionic polymer PVA and anionic CG, a water-soluble extractive of sulfated polysaccharides from red algae were chosen to modify the CNC suspensions. They were mixed with CNC suspensions for easier coating application. For comparison, both cast and coated CNC films were prepared as the inner oxygen barrier layer. The optical, barrier, and mechanical properties of multilayer films were characterized. This bio-based, biodegradable, and recyclable film creates an enormous commercial potential for food packaging applications.

2. Materials and methods

2.1. Materials

A 10.3 wt% CNC suspension (labeled as 10% CNC) was produced by the Forest Products Laboratory (Madison, WI). PVA powder with an average M_w of 130 K and 99 + % hydrolyzed and CG powder were purchased from Sigma-Aldrich (St. Louis, Missouri, USA) and Fisher Scientific (Hampton, New Hampshire, USA), respectively. A PLA film roll (NATIVIA® NTSS 40, thickness of 40 μm) was purchased through Taghleef Industries LLC (Newark, Delaware, USA). This PLA film certified TÜV AUSTRIA (four-star certification) OK biobased (S206), DIN EN 13432 (7H0052) for compostable intermediates, and complies with EU and FDA food contact regulations. All materials were used without further modification.

2.2. Preparation of CNC-PVA and CNC-CG formulations

Five grams of PVA powder were mixed with 95 g water at about

80–90 °C under heating and stirring to obtain a 5 wt% clear PVA solution. A 3 wt% CG solution was prepared by dissolving 3 g κ-carrageenan powder into 97 g water at 70 °C under magnetic stirring. Various amounts of the 5 wt% PVA or 3 wt% CG solutions were added into a 6 wt % CNC suspension to make four 6% CNC formulations with 10% and 15% PVA or 10% and 15% CG based on the CNC solid content. In summary, 8 solutions or suspensions were prepared and labeled as 10% CNC, 6% CNC, 5% PVA (neat), 3% CG (neat), 10% PVA-CNC (6% CNC+10% PVA on CNC basis), 15% PVA-CNC (6% CNC+15% PVA on CNC basis), 10% CG-CNC (6% CNC+10% CG on CNC basis), and 15% CG-CNC (6% CNC+15% CG on CNC basis). The formulations were fully mixed by a planetary centrifugal mixer (ARE-310, Thinky Corporation, Tokyo, Japan) at 2000 rpm for 2 min, followed by 30 s degassing.

2.3. Rheological characterization

Rheological measurements were carried out using a hybrid rheometer (DHR-3, TA Instruments) equipped with a Peltier plate and a Peltier concentric cylinder temperature system. The steady-state viscosities of samples were obtained by flow sweep tests with increasing shear rates from 0.1 to 100 s^{-1}. Strain sweep tests were carried out with 10 rad s^{-1} angular frequency and strain varying from 0.1 to 100% to determine the linear viscoelastic region. The dynamic shear tests were then performed under angular frequency changing from 100 to 0.1 rad s^{-1} at the determined strain. Experiments on 6% CNC, 10% CNC, 10% CG-CNC, and 15% CG-CNC suspensions were conducted using a cone-plate geometry (diameter: 40.0 mm, angle: 2°). In the case of 10% and 15% PVA-CNC suspensions, experiments were performed using a cup and bob geometry. All the rheological tests were performed at 23 °C.

2.4. Surface tension measurements

The surface tension of different formulations was measured using a high-precision tensiometer (K100SF, KRÜSS Scientific, Hamburg, Germany) according to the Wilhelmy plate method (Wu et al., 1999). A standard Wilhelmy plate was vertically immersed in the dispersions. The surface tension can be related to the force applied on the plate by Eq. (1):

$$F = P\gamma\cos\theta - \rho Ahg \quad (1)$$

Where F is the detected force, P the wetted perimeter of the plate, γ the surface tension of the probe liquid, θ the liquid-solid-air contact angle, ρ the probe liquid density, A the cross-sectional area of the plate, h the immersion depth, and g the gravitational constant. The two terms on the right-hand side of Eq. (1) correspond to the wetting force and the buoyancy force, respectively.

This measurement was completed by RISE Research Institutes of Sweden (Stockholm, Sweden). Each measurement was performed at least for 5 min and 20 data points collection and at least two measurements were done for each dispersion.

2.5. Film coating and lamination

CNC suspension alone or prepared CNC-based suspensions were coated on the PLA film manually. Two different rods, #22 (8.2 mm diameter) and #52 (15.4 mm diameter) from the BYK-Gardner 2101 automatic film applicator (Columbia, MD, USA) were used to control the coating thickness. The larger rod number produces a thicker coating layer. After drying at room temperature, the coated PLA films were laminated with another piece of PLA film in a hot-roll laminator (HL-200, ChemInstruments, Fairfield, OH, USA) to obtain the PLA-CNC-PLA laminate structure, as illustrated in Fig. 1. The lamination was carried out at 90 °C and 0.276 MPa nip pressure with a speed of 50 cm min^{-1}. Besides coated CNC film in the middle layer, laminates of PLA-casted CNC film-PLA were also prepared for comparison. Neat free-standing CNC films were fabricated with a 2 wt% CNC suspension (15% sorbitol based on the solid of CNCs added as plasticizer) in a Petri dish through the solvent-casting method. Free-standing CNC film preparation details were detailed in our previous study (Chen et al., 2022). All fabricated samples were stored at a 23 °C and 50% RH condition room before testing the properties.

2.6. Optical properties of films

Light transmittance of coated and laminated films was obtained using a UV−vis spectrometer (Ocean Optics USB2000 +, Orlando, FL, USA) including a DH-2000 light source (190 – 800 nm). The optical transmittance at 550 nm was reported. The coating surface of CNC formulations on PLA substrate was revealed by a polarized optical microscope (POM) (Nikon Eclipse LV100 POL, Tokyo, Japan). A 530 nm retardation plate was added to enhance the birefringence.

The microstructure of the coating surface and cross sections of multilayer laminated films were analyzed by a field-emission scanning electron microscope (FE-SEM) (Zeiss NVision 40, Jena, Germany). Before imaging, a 4 nm gold-palladium conductive layer was sputter-coated on the surface or cross-section.

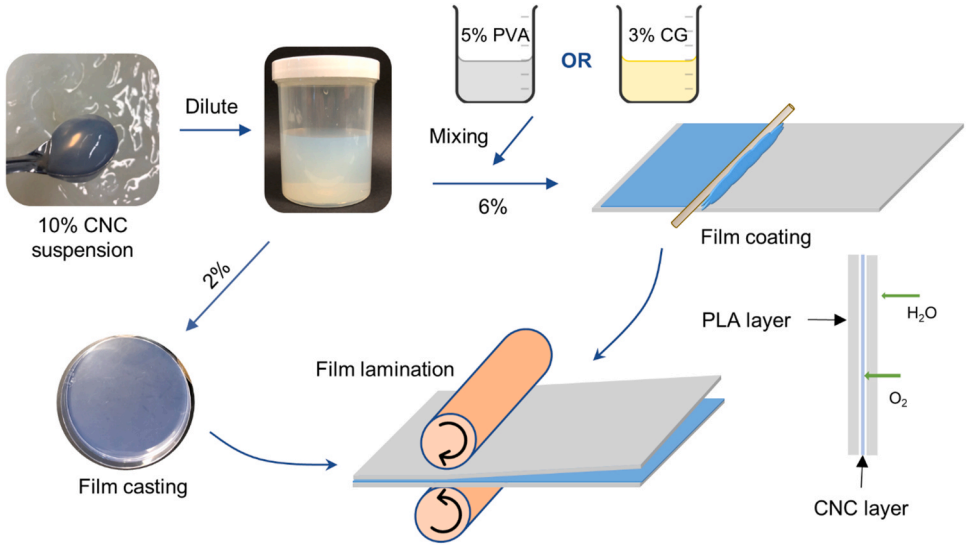

Fig. 1. Schematic illustration of the laminated PLA-CNC-PLA film fabrication.

2.7. Gas barrier properties of films

The gas barrier properties of the laminated films were evaluated by water vapor and oxygen transmission rate and permeability. The water vapor transmission rate (WVTR) and water vapor permeability (WVP) of films were measured according to the ASTM E96/E96M-16 standard. Briefly, a circular sample with a 7 cm diameter was sealed on the top of a Mason jar with 50 g distilled water inside and placed in the conditioning room (23 °C and 50% RH). The WVTR and WVP were calculated based on the weight changing over time (1, 2, 3, 4, 5, 6, 7, 10, and 15 days) using Eqs. (2) and (3), respectively:

$$WVTR(g \quad m^{-2} \quad day^{-1}) = (G/t)/A \tag{2}$$

Where G is the weight change, t is the time, and G/t is the slope of the line in the mass change-time curve (Fig. S4); A is the test area of the film.

$$WVP \quad (g\mu m \quad m^{-2} \quad day^{-1}kPa^{-1}) = \frac{WVTR \times l}{S \times \Delta_{RH}} \tag{3}$$

Where S is the water saturation vapor pressure at 23 °C (2.81 kPa); l is the thickness of the film; Δ_{RH} is RH difference (100%−50%) cross the film.

The OTR results were obtained by a MOCON oxygen permeation analyzer (OX-TRAN 2/22, Minneapolis, MN, USA) with a 5.64 cm^2 testing area cartridge according to the ASTM F1927 standard. OP results were calculated by the Eq. (4):

$$OP(cm^3\mu m \quad m^{-2} \quad day^{-1}atm^{-1}) = OTR \times l/P \tag{4}$$

Where P indicates the oxygen partial pressure difference of the film; l is the thickness of the film.

The oxygen barrier performance was conducted at 23 °C and 50% RH in both the carrier and testing gases. Three replicates of each sample type were completed for barrier testing.

2.8. Mechanical properties of films

An Instron 5942 universal testing system with a 500 N load cell (Instron, Norwood, MA, USA) was used for determining the tensile strength, Young's modulus, strain at break, and toughness of laminated films. For tensile testing, films were cut into 50 mm × 10 mm specimens. The initial gauge length and crosshead speed were 20 mm and 3 mm min^{-1}, respectively. Six measurements were carried out for average result calculation. Toughness was determined from the area under the stress-strain curve and was integrated by a MATLAB code.

The tear resistance of the laminated films was examined via a Lorentzen & Wettre tearing tester (ABB Ltd, Stockholm, Sweden) according to the TAPPI T 414 Elmendorf method. A Type A pendulum with 800 gf capacity was used for measurement. Two pieces of each specimen with 63 mm width were torn together to reach the applicable pendulum capacity. Tear resistance was performed initially by knife cutting. Five repeats were completed per sample.

2.9. Statistical analysis

Data were analyzed using one-way analysis of variance (ANOVA) using a Tukey test based on 95% confidence intervals. Software IBM SPSS V28 (IBM Corp., Armonk, NY, USA) was used for statistical analysis.

3. Results and discussion

3.1. Characterization of CNC-based coating formulations

The appearance of the neat CNC suspensions and the mixed CNC suspensions with PVA or CG can be observed in Fig. 2a and b. Fig. 2b shows behavior of suspensions after 1 day inverted standing to visually reflect the viscosity difference among suspensions. The original 10.3 wt % CNC suspension displayed a solid-like behavior with high viscosity and did not flow down after 1 day of inversion standing in a vial (Fig. 2b). When the 10% CNC suspension was diluted to 6 wt%, it became semi-transparent and started to flow immediately, which indicated a state conversion from being solid-like to liquid-like and remarkably decreasing of viscosity. Adding 10% or 15% PVA did not apparently change the appearance or flow behavior of the suspensions visually. However, significant differences were observed when 10% or 15% CG was added into a 6% CNC suspension. The color of the mixed suspensions changed to milky white. This color change could be attributed to the light scattering caused by the gelling effect of the large molecular weight carrageenan in the CG-CNC suspensions (Chen et al., 2023). The viscosity of the suspensions increased remarkably. Only a trace amount of the 10% CG-CNC suspension flowed down after 10 min inversion standing (Fig. 3e). There was no apparent movement of the 15% CG-CNC suspension after the 1-day settlement (Fig. 2b). The specific viscosity results are discussed as follows.

The rheological properties of the suspensions are a crucial factor related to the film coating quality such as uniformity, continuity, and thickness. Fig. 2c shows the steady-state viscosity as a function of the shear rate for the 5% neat PVA solution, neat CNC suspensions, and CNC with PVA or CG composite formulations. Different rheological behaviors are observed for the samples. The neat 10% CNC suspension had a high

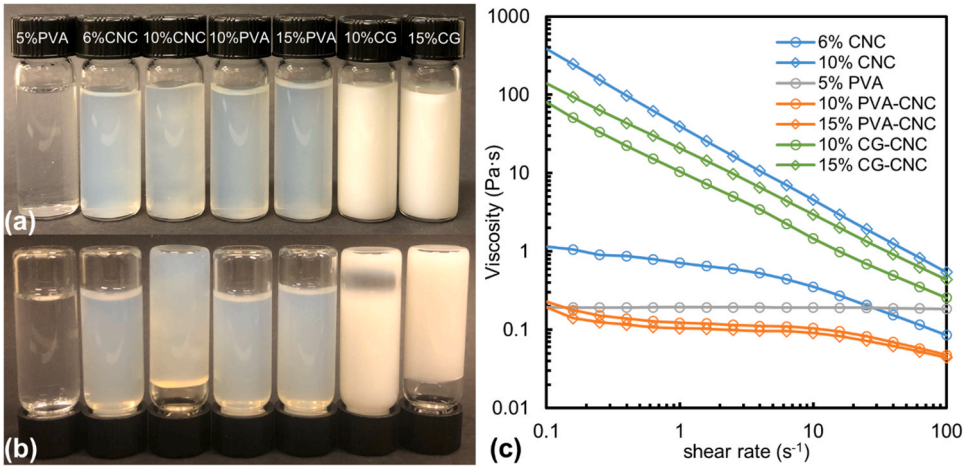

Fig. 2. The photographs of different formulations (a), and after 1 day (b) vials inversion; the steady-state viscosity of coating formulations as a function of shear rate from flow sweep tests (c).

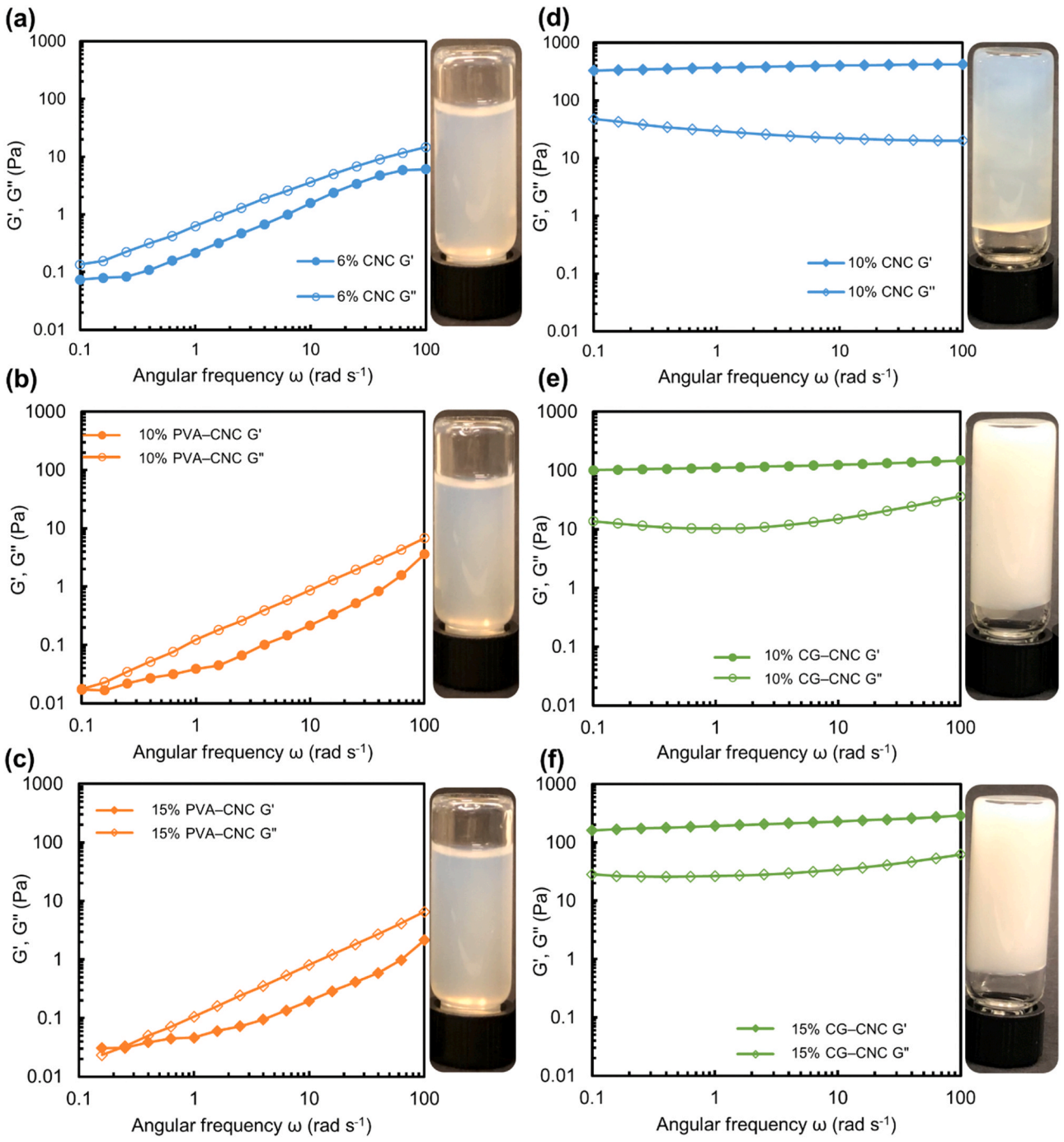

Fig. 3. Shear storage modulus (G′) and loss modulus (G″) from dynamic tests and the pictures after 0 or 10 min inverted standing: the (a) 6% CNC, (b) 10% PVA-CNC, and (c) 15% PVA-CNC suspensions exhibited $G' < G''$ liquid-like behavior and fell off instantly after inverted standing; the (d) 10% CNC, (e) 10% CG-CNC, and (f) 15% CG-CNC suspensions exhibited $G' > G''$ solid-like behavior and did not apparently fall off after 10 min inverted standing.

initial viscosity of 387 Pa·s at the shear rate of 0.1 s^{-1}. The viscosity decreased drastically to around 1 Pa·s when the CNC suspension was diluted to 6%. The 5% neat PVA solution has a relatively low flat viscosity and displays Newtonian behavior over all shear rates at 23 °C. Thus, adding PVA into CNC led to a further declination in viscosity of the 6% CNC suspension, indicating a possible lubrication effect where PVA enables the surfaces of CNCs to slip past each other more easily (Nuruddin et al., 2021). Whereas CG significantly increased the viscosity of the 6% CNC suspension to 81 Pa·s and 140 Pa·s with 10% and 15% mixing content, respectively. The viscosity results are consistent with the suspension inversion performance in Fig. 2b.

The 10% CNC, 10% and 15% CG-CNC suspensions exhibited steep increases in viscosities at low shear rates, which is the manifestation of network formation in the samples and characteristic of a yield behavior (Fig. 2c). The viscosity of the 6% CNC suspension remained relatively Newtonian at the low shear rates and exhibited a shear thinning behavior at the high shear rates. The viscosity curves of the 10% and 15% PVA-CNC suspensions have a small upturn section towards the low shear rates (Fig. 2c), indicating network formation to some extent, or some weak associations between nanocrystals. After the upturn, the viscosity behaves like that of the 6% CNC suspension towards the high shear rates. The differences among the viscosities of this group and those

of the group of 10% CNC and 10% and 15% CG-CNC become larger towards low shear rates, indicating different structures of the suspensions at rest between the two groups (Xu et al., 2017).

The rheological behavior of different suspensions was further characterized by dynamic shear experiments. Fig. 3 shows shear storage modulus (G′) and loss modulus (G″) of the suspensions from dynamic tests and the pictures after 0- or 10-min inverted standing. The 6% CNC (Fig. 3a), 10% PVA-CNC (Fig. 3b), and 15% PVA-CNC (Fig. 3c) suspensions exhibited the behavior of a viscoelastic liquid where the loss modulus is higher than the storage modulus ($G'' > G'$) and fell off immediately after inverted standing. Similar behavior was also observed by Ureña-Benavides et al. (2011) at 7.69 to 10.4 vol% CNC concentration (Ureña-Benavides *et al.* 2011). Additionally, there exists a crossover point of dynamic moduli at the low frequencies for the 10% and 15% PVA-CNC suspensions (Fig. 3b and c). This is the manifestation of network formation in the samples, which is consistent with steady state viscosity results in Fig. 2c. The 10% CNC (Fig. 3d), 10% CG-CNC (Fig. 3e), and 15% CG-CNC (Fig. 3 f) suspensions exhibited relatively larger flat shear moduli than those of 6% CNC, 10% and 15% PVA-CNC, where the storage modulus is higher than the loss modulus ($G' > G''$) indicating the solid-like behavior of the samples and the suspensions did not apparently fall off after 10 min inverted standing.

Besides rheological properties, the compatibility between substrates and coating formulations is another important aspect of coating processing (Chowdhury et al., 2018), especially between hydrophobic polymers and hydrophilic natural materials. The surface energy of the purchased PLA film is 37 mN/m. The surface tension of fabricated formulations is as follows in mN/m: 10% CNC, 77.70; 6% CNC, 73.43; 5% PVA, 39.01; 10% PVA-CNC, 48.82; 15% PVA-CNC, 46.34; 10% CG-CNC, 74.71; 15% CG-CNC, 79.42 (Table S1). Undoubtedly, the CNC neat and CNC mixed with CG suspensions show a higher surface tension than water at 72.8 mN/m, behaving like that the surface tension of water is increased when salt is added to it, since both CNCs and CG, like salts, can immobilize water molecules around them This consequently causes a visible problem when coating CNC suspensions onto the PLA films. The 6% CNC suspensions cannot evenly spread out on the PLA surface (Fig. S1a). Although the 10% CNC suspension could be coated on the PLA films attributed to its high viscosity, a continuous wet CNC film would not be obtained (Fig. S1b). The 15% CG-CNC formulation could produce a continuous coating surface (Fig. S1f) even with a high surface tension value; this is probably because of its high viscosity (Fig. 2a).

Because PVA is also a hydrophilic polymer, it would be unexpected that adding PVA into water or CNC suspensions at the test levels decreased the surface tension. However, this finding agrees with the literature. PVA has an amphiphilic nature with alternating hydrophobic methylene and hydrophilic hydroxyl groups. In the diluted regime, it has been observed that PVA behaves like a surfactant and decreases the surface tension of water with increasing polymer concentration (Bhattacharya & Ray, 2004; Moll et al., 2018) up to ~4 wt% PVA (neat) concentrations, and then increases the surface tension with polymer concentration until around 10 wt% (neat), at which the surface tension of the PVA solution is similar to that of pure water (Rošic et al., 2013). Consequently, adding a small amount of PVA into CNC suspensions could significantly improve the quality of coating. The higher PVA concentration (15%) displayed a better coating ability (Fig. S1c and d). Based on the coating performance of different formulations, the 15% PVA-CNC and 15% CG-CNC mixed suspensions were selected for further evaluation. In addition, two different coating rods, #22 and #52 were used to estimate the effect of coating thickness on the film properties. The #22 rod produces a coating thickness of 2–3 μm, while the #52 rod led to a relatively thicker coating layer of 5–6 μm. After coating, another layer of PLA film was attached to the coated surface to fabricate a three-layer sandwich structure film. Laminated samples are labeled with L and abbreviations of each group are listed in Table S2.

3.2. Morphology of coating surface and laminated films

Morphological images collected by FE-SEM provide more microscopic information on the PLA film and CNC coating surfaces. Generally, the PLA film exhibits a smooth surface (Fig. 4a). When coated with the 15% PVA (Fig. 4b) or the 15% CG (Fig. 4c) suspensions, the surface exhibited apparent microstructure and roughness. At 20 k magnification, nanocrystals can be observed either in the 15% PVA (Fig. 4e) or 15% CG (Fig. 4 f) coating surfaces and appear to be arranged together tightly. Fig. 4g-i depict the cross-section of the laminated multilayer films. It can be observed they are a three-layer structure with a casted CNC film or coated composite CNC layer in the middle sandwiched by two PLA layers, and the coated composite CNC layers are much thinner than the cast CNC film.

3.3. Optical performance

POM images revealed the morphology of the air-dried surface of the CNC coatings on PLA films (Fig. 5). The POM image of the purchased PLA film (Fig. 5a) does not show apparent birefringence phenomenon, indicating no evidence of spherulitic crystalline structures existing (Takkalkar et al., 2019). The surface morphology of the 10% CNC suspension coating (Fig. 5b) is different from that of cast CNC films (Fig. S2). To compare with the cast samples, the difference was presumably ascribed to the very thin coating thickness (~2 μm), high initial suspension concentration, fast drying process, and shear stress from the coating rod, which changed the degree of orientation for chiral nematic CNC from isotropic to an anisotropic structure (Chowdhury, Nuruddin, et al., 2018). In terms of the effect of coating rod size on the CNC orientation, it seems that the smaller rod produced more oriented CNC along the coating direction. Compared to pure CNC suspensions, the CNC-PVA compositions showed a more oriented arrangement (Fig. 5c and d), turning from partially parallel to partially perpendicular to the shear direction as the coating thickness increased (Fig. 5d). A coarser texture was found on the CNC-CG coating surfaces. The 45° arrangement direction can be easily observed when coated by a #22 rod (Fig. 5e), but this is not obvious when using a #52 coating rod (Fig. 5 f).

Transparency is an essential parameter in many food packaging applications, which allows consumers to have a visible inspection of the contents. The transmittance of PLA film, CNC-coated PLA films, and PLA-CNC-PLA laminated films at the range from 400 to 800 nm are presented in Fig. S3 and Fig. 6a. Pristine PLA is the clearest and most transparent film, which has 98% transmittance at 550 nm. The coatings with the CNC-CG did not reduce the transparency remarkably, however, the light transmittance decreased to 71% when coated with the CNC-PVA composites (Fig. S3). This was owing to light scattering caused by PVA polymer chains commingled with CNC particles. After lamination, all films exhibited a great visual appearance with transmittance above 77% and this can be observed in the photographs of the pure PLA and laminated films on their printed designations in Fig. 6b. Among these films, the PLA laminate of two PLA films reduced the transmittance to 80%; the transparency of the PLA-CG laminated films also reduced compared with the coated PLA-CG films. In contrast, the light transparency of the laminated PLA-PVA films increased to around 80% compared to their coated films. Moreover, film transparency did not change significantly ($P > 0.05$) in the two-coating thickness of CNC-PVA and CNC-CG formulations after lamination (Fig. 6a insert).

3.4. Barrier properties

The impact of preparation methods (casting or coating CNC film), CNC formulations (15% PVA or 15% CG), and coating thickness (#22 and #52 rods) on laminated PLA-CNC-PLA films' barrier properties were evaluated by WVTR, WVP, OTR, and OP (Fig. 7). Neat CNC films were prepared by casting and drying a CNC suspension in Petri dishes and were then laminated with PLA films on both sides (LCNC group). PLA is

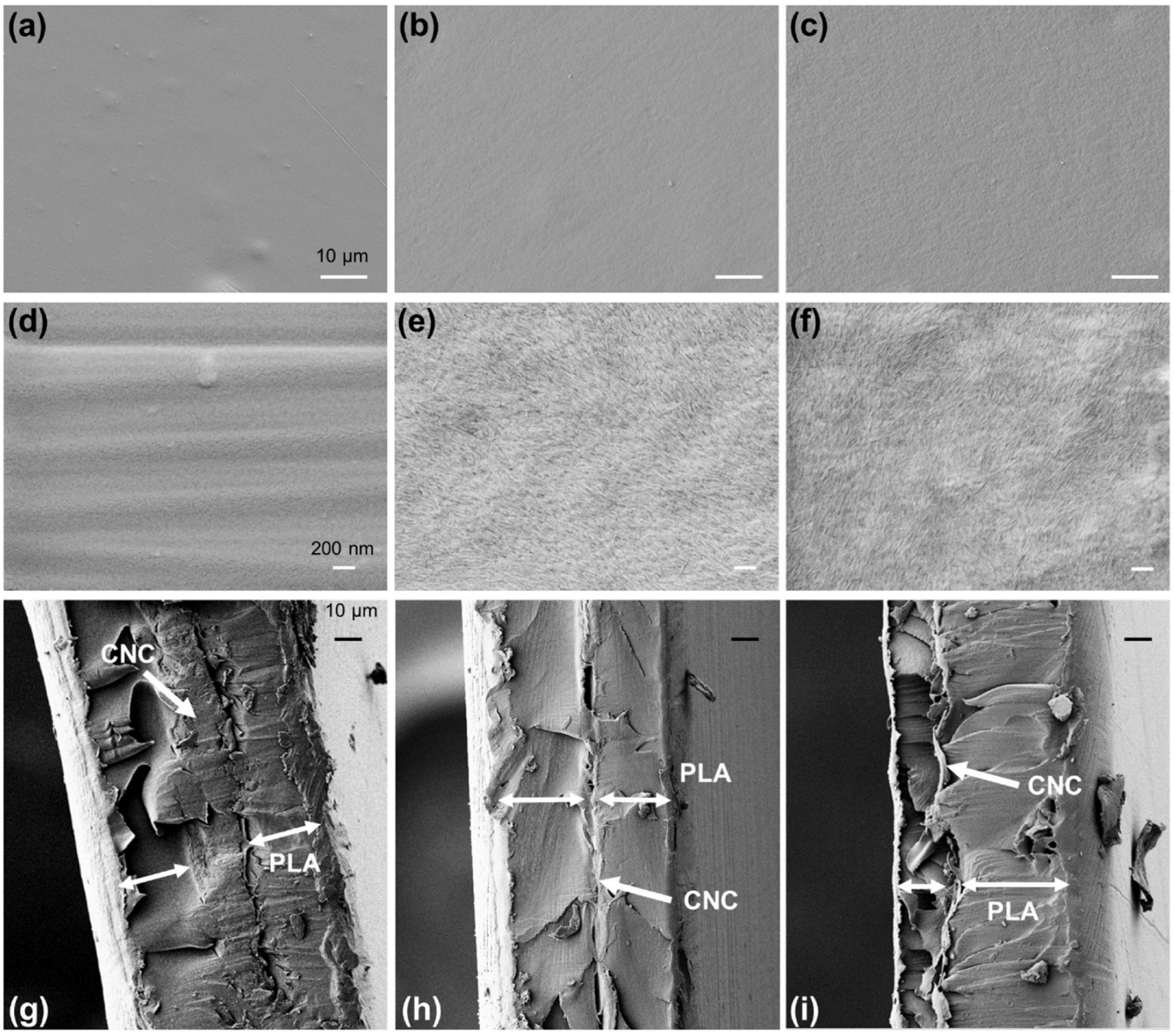

Fig. 4. The surface morphology of the original PLA film (a, d), the 15% PVA coating (b, e), and 15% CG coating (c, f) at 1000x and 20,000x magnification, respectively. The cross-section images of the laminates of PLA-casted CNC-PLA (LCNC) (g), PLA-coated 15% PVA with rod #22-PLA (LPVA#22) (h), and PLA-coated 15% CG with rod #22-PLA (LCG#22) (i).

an as-received film without any treatment or processing, while LPLA is a laminated film of two PLA films without a CNC core layer. The other four groups in Fig. 7 were all prepared by coating CNC-based formulations (CNC with 15% PVA or CG) on PLA films, followed by laminating another layer of PLA on the coating side.

The water barrier properties of films are evaluated through WVTR and WVP. The neat CNC film does not have outstanding water barrier performance with a WVTR of 460 g m^{-2} day^{-1} (Fig. 7a). This is ascribed to the hydrophilicity of the CNC films. The interaction among CNCs is mainly hydrogen bonding formed by their surface hydroxyl groups, which could be weakened easily by water molecules. The water barrier is considerably improved when CNC film is protected with PLA film on the outside as compared with the neat CNC film. The WVTR values of all sandwich-structured films drop to around 23 g m^{-2} day^{-1}, 20 times lower than that of the pure CNC film and at the same order of magnitude as that of the double layered LPLA, which indicates the water barrier properties of laminated films are dominated by the water barrier capability of the outside PLA films. Therefore, there are no large differences among all the laminated films. Permeability results, shown in Fig. 7, are normalized transmission rates with sample thickness and the pressure difference across the test sample. The WVP of the CNC film is 9603 g μm m^{-2} day^{-1} kPa^{-1}, belonging to the poor water barrier grade. PLA laminated CNC films could be classified as the low grade attributable to the WVP smaller than 3000 g μm m^{-2} day^{-1} kPa^{-1} (Wang et al., 2018).

The OTR of CNC and multilayer films at 50% RH are shown in Fig. 7c. Although the PLA film prevents CNC film from deteriorating in water, the oxygen barrier properties themselves are insufficient. This is illustrated in Fig. 7c and d, where the OTR of single layer and laminated PLA is 344 and 161 cm^3 m^{-2} day^{-1}, respectively. The PLA is a low oxygen barrier film based on the OP results, which is between 4000 to 40,000 cm^3 μm m^{-2} day^{-1} atm^{-1} (Wang et al., 2018). Cellulose nanomaterials usually exhibit excellent oxygen barrier properties, owing to their high crystalline domains, strong hydrogen bonding among cellulose molecules, and tight packing among nanocrystals to block gas molecules or deflect the gas passing paths in the films. The OTR of the

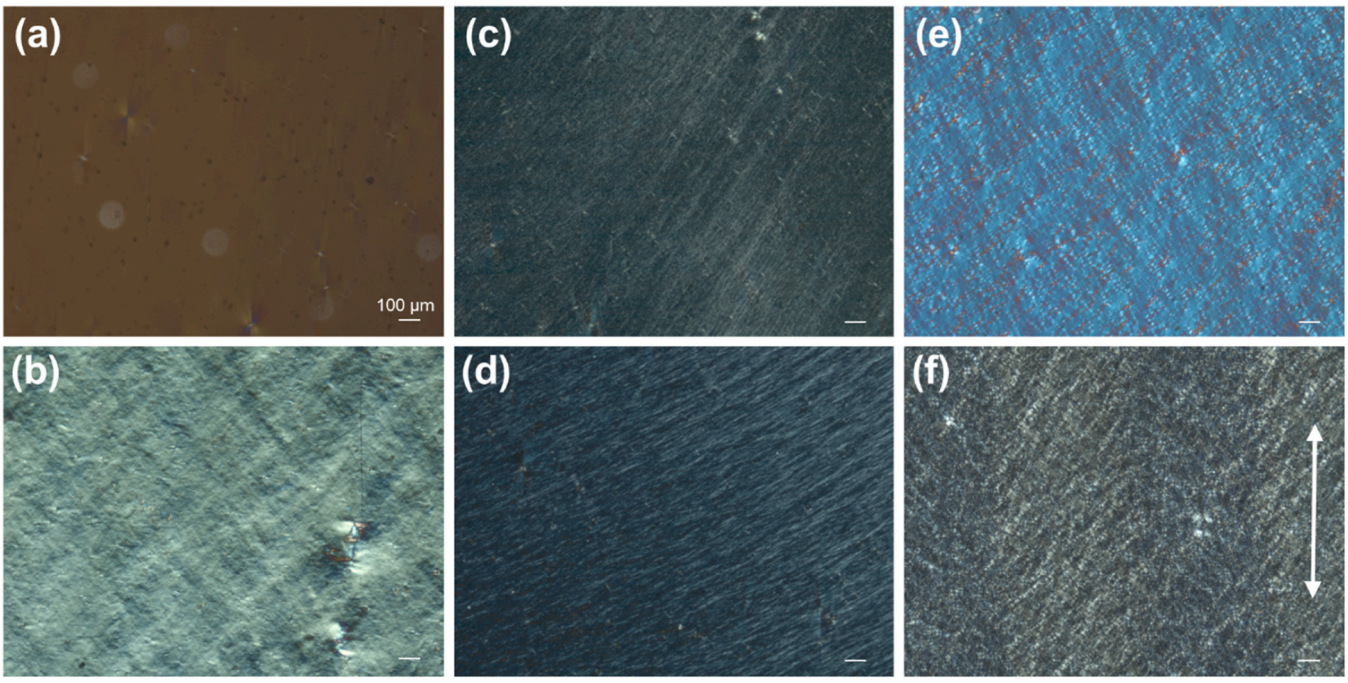

Fig. 5. Polarized optical microscope (POM) images of the surfaces of the PLA film (a), the coatings of the 10% CNC (b), 15% PVA Rod #22 (c), 15% PVA Rod #52 (d), 15% CG Rod #22 (e), and 15% CG Rod #52 (f). The arrow indicates the coating direction for all images.

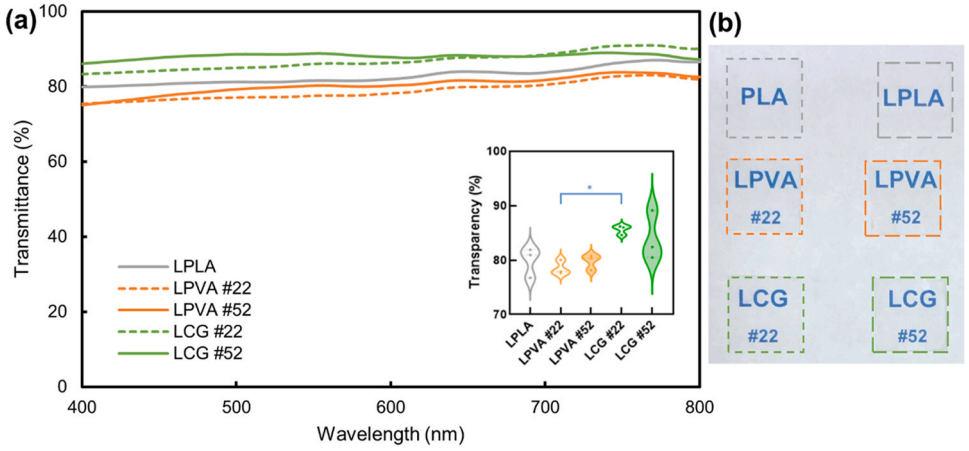

Fig. 6. Optical transparency of laminated films over the 400–800 nm spectrum (a), and photographs of transparent films.

casted CNC film is only 1.6 cm^3 m^{-2} day^{-1} at 50% RH. Accordingly, a CNC layer was laminated between two PLA films to improve their oxygen barrier properties while taking advantage of PVA water barrier capability. The OTR of PLA film significantly decreased to 4.4 and 60 cm^3 m^{-2} day^{-1} by coating with CNC-PVA #22 and CNC-CG #22 layer. The OTR further declined when coated with a thicker CNC layer (LPVA #52). Meanwhile, the OTR of LPVA #52 (2.2 cm^3 m^{-2} day^{-1}) is comparable to the LCNC film (1.7 cm^3 m^{-2} day^{-1}). However, the thickness of the CNC coating layer was only 5 μm, appreciably thinner than the cast film of 30 μm. Therefore, the coating method is much more economical than the casting method in preparing sandwich-structure films. Thus, in this type of sandwiched film, PLA and CNC films have a synergistic effect on the barrier properties of multilayer food packaging: the outside PLA films reduce the water impact on the core CNC film, meanwhile, the core CNC layer can block oxygen molecules transmission.

3.5. Mechanical properties

Good vapor and gas barrier performance can preserve packaged food against external contamination. Mechanical properties are another crucial factor in protecting food from outside physical damage or avoiding packaging film failure during transportation or storage (Marsh & Bugusu, 2007). The results of PLA and PLA laminated films are summarized in Fig. 8. The tensile strength, strain at break, and elastic modulus of the as-received PLA film are 69.0 MPa, 4.2%, and 2.6 GPa, respectively, which are in the range of previously reported results (Auras et al., 2003; Muller et al., 2017). When laminating two pieces of PLA films together, the tensile strength and stiffness increased to 78 MPa and 3.5 GPa, respectively, but the strain value decreased to 3.33%, which might be ascribed to increased crystallization after the lamination at 90 °C. After incorporating CNC films (both CNC-PVA and CNC-CG coating compositions) into the laminated structure, the tensile strength does not significantly change. The tensile strength of plastic-CNM multilayer films is usually governed by the base plastic

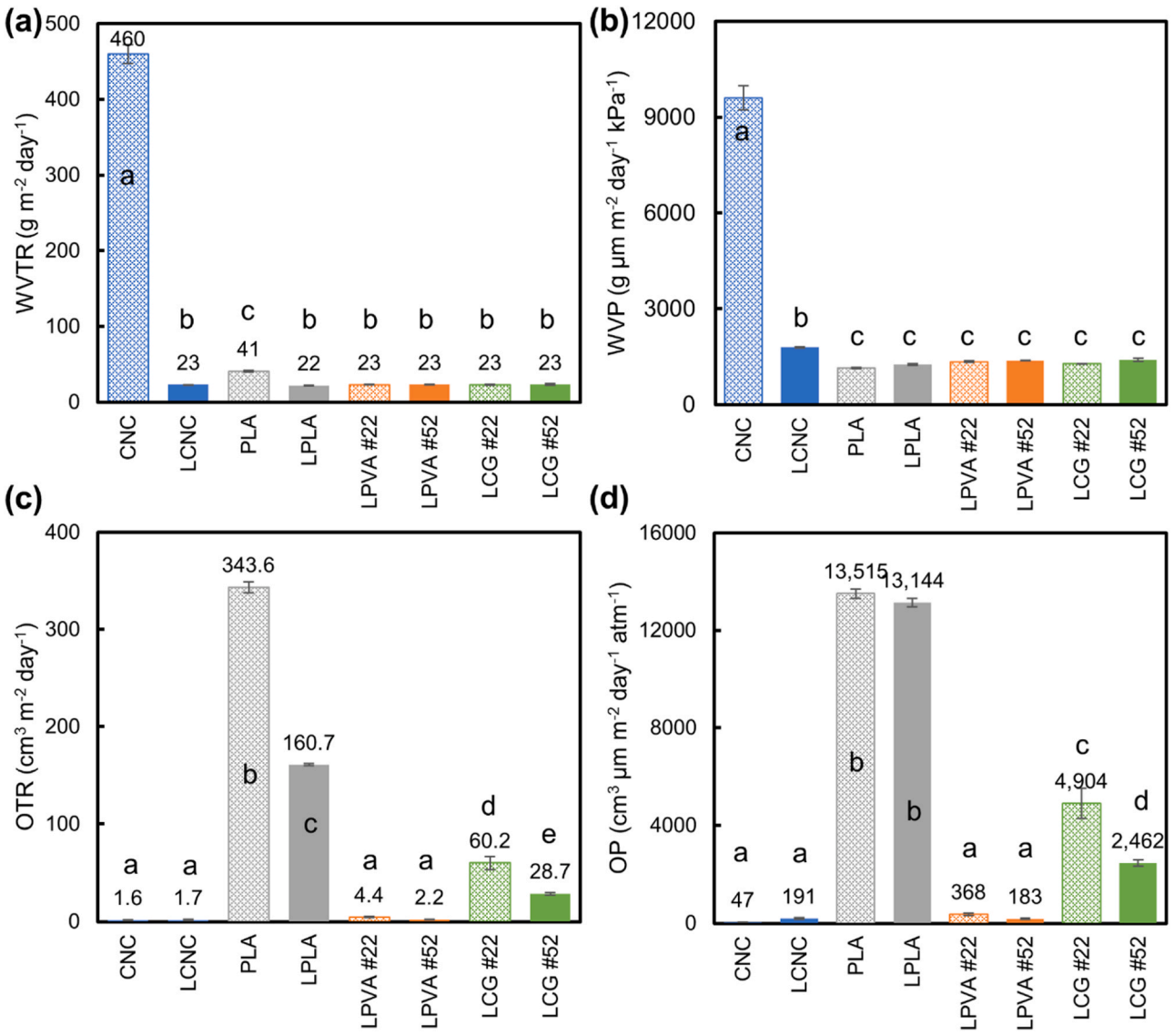

Fig. 7. Barrier properties of the CNC and laminated films: Water vapor transmission rate (WVTR) (a) and water vapor permeability (WVP) (b) under 23 °C and 100%/50% RH across the sample; oxygen transmission rate (OTR) (c) and oxygen permeability (OP) (d) under 23 °C and 50% RH. The letters labeled on the column charts are statistical results.

films, not by the core CNC layer (Wang, Chen, et al., 2020). Thereby, the strength of laminated PLA-CNC films was improved by 63% compared to a free-standing CNC film with sorbitol as the plasticizer (Chen et al., 2022). The strain and toughness of the laminated PLA films were improved by adding CNC composite layers, especially for the LCG film (Fig. 8d). This increase could be attributed to the additives, which can improve the toughness of the films (Chen et al., 2023). However, the stiffness and strength of the LCG film decreased as shown in Fig. 8a and b. The large variations in the tensile strength of the PLA and laminated LPLA films might be ascribed to the anisotropic nature of PLA films in machine and cross directions and the composition with an isotropic CNC layer reduced the variations (Fig. 8a).

Although tensile-related properties are one of the most crucial aspects to reflect the mechanical performance of food packaging, tear resistance cannot be ignored. Generally, the tensile strength of CNC films can be improved remarkably with an appropriate plasticizer, but they may be still too fragile to handle and use directly during packaging manufacturing. For example, a neat CNC film is easily torn (Fig. S5b). This problem could be resolved by laminating CNC film with plastics as displayed in Fig. S5a. The CNC film showed low tear resistance with 10.1 gf. As expected, the tear strength of the CNC film was improved considerably when laminated with PLA films. The tear strength of LPVA #22, LPVA #52, LCG #22, and LCG #52 were 115.6, 125.7, 123.2, and 124.8 gf, respectively. The tear performance of PLA-CNC multilayer films demonstrated that PLA film could indeed protect the inner weak CNC film against ambient mechanical damage.

3.6. *Water resistance and recycling*

Furthermore, neat CNC films are extremely sensitive to water damage. They begin to disintegrate immediately when they are immersed in water (Chen et al., 2022). Placed on a neat CNC film, a drop of water soon penetrates the film and leaves the underlying area appearing like a hole (Fig. S6b). This is another reason why CNC films cannot be used alone. Accordingly, water-repellent polymer films were used to prevent CNC films from water damage. Fig. 9 shows that the water damage on CNC films was greatly retarded after laminating them with PLA films. After soaking in water for 2 h, only the edge area of the laminated films was affected by water, as evidenced by the iridescent color of the cast CNC film in the central area (Fig. 9a). It was observed that sandwiched

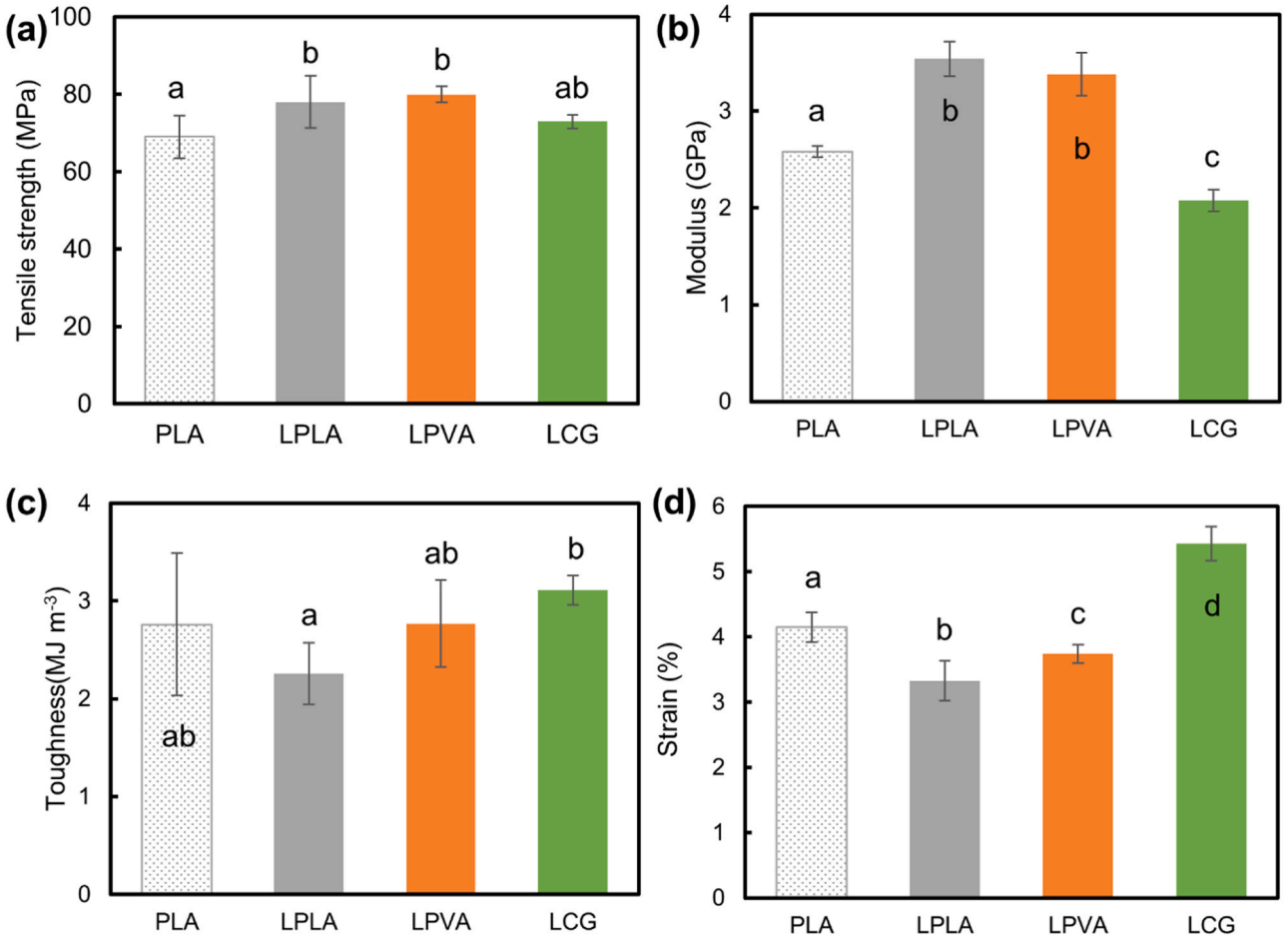

Fig. 8. Mechanical properties of the PLA film and laminated films: tensile strength (a), Young's modulus (b), toughness (c), and strain at break (d).

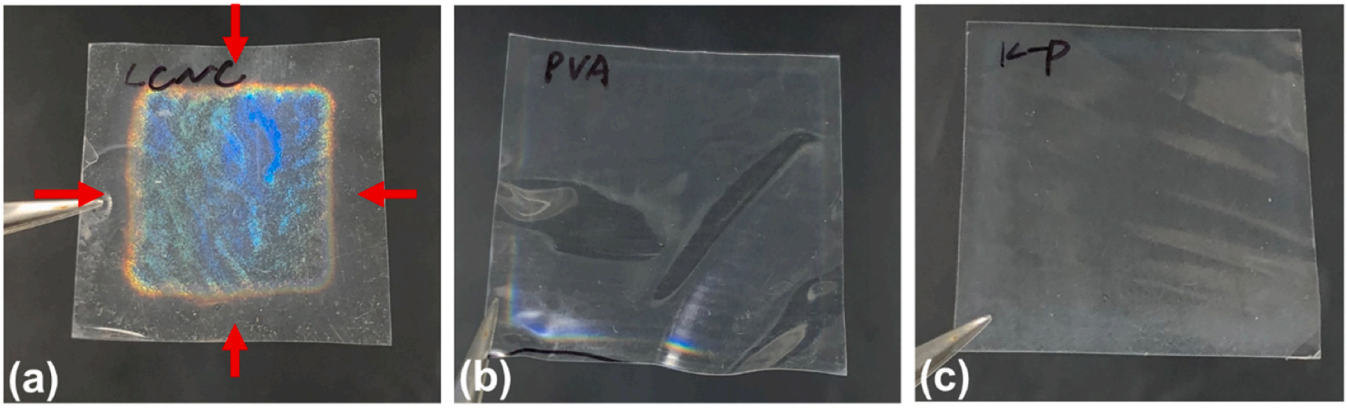

Fig. 9. Laminate films: LCNC (a), LPVA (b), and LCG (c) after 2 h soaking in water.

films with a coated CNC layer show better water protection than those with a cast CNC layer, attributed to a thinner CNC layer and a more compact laminate structure. On the other hand, the edge area of the multilayer films delaminated after the interlayer CNCs dissolved into water. Consequently, the laminated PLA films could be easily separated leading to improved recyclability. From this perspective, fabricated multilayer lamination films can help eliminate or delay food packaging entry into the waste stream.

4. Conclusions

In this work, eco-friendly food packaging films with high performance were fabricated with CNC-based suspensions and PLA films in a facile way. The prepared CNC-based formulations were properly coated on the PLA substrate, followed by another layer of PLA film lamination to form a multilayer structure. It was demonstrated that nonionic polymer PVA can decrease the surface tension and viscosity of CNC suspensions, while the anionic CG can increase the viscosity. Both formulations, whether mixing with PVA or CG, significantly improved CNC processability and coating ability on plastic films. The multilayer films

showed high light transparency (higher than 77%) and excellent moisture and oxygen barrier properties, attributed to the synergistic effect of PLA and CNC layers. The tear and water resistance were significantly improved compared with neat CNC films. Moreover, there was no adhesive or tie layer in these multilayer films, thus, enabling the materials to be more easily recycled after use. A laminate structure of PLA and CNCs fits well into the concept of a circular economy by reusing, recycling, and upcycling, contributing to a more sustainable world. Additionally, coating and lamination technology have already been commercially used in the food packaging field (Coles et al., 2003), which highly improves the possibility of scaling up this PLA-CNC-PLA film in the future.

CRediT authorship contribution statement

Gardner Douglas Jerome: Conceptualization, Funding acquisition, Resources, Supervision, Writing – review & editing. **Shams Es-haghi Siamak:** Methodology, Writing – review & editing. **Wang Lu:** Conceptualization, Methodology, Writing – review & editing. **Wang Jinwu:** Conceptualization, Funding acquisition, Resources, Supervision, Writing – review & editing. **Tajvidi Mehdi:** Methodology, Resources, Writing – review & editing. **Chen Cong:** Conceptualization, Formal analysis, Investigation, Methodology, Visualization, Writing – original draft.

Declaration of Competing Interest

The authors declare that they have no known competing financial interests or personal relationships that could have appeared to influence the work reported in this paper.

Data availability

Data will be made available on request.

Acknowledgements

This work was supported by the Agriculture and Food Research Initiative Foundational and Applied Science Program grant no. 2018–67010-27906 from the USDA National Institute of Food and Agriculture. The authors gratefully acknowledge the University of Maine Electron Microscope Laboratory for their support and assistance in this work and Dr. Maziar Sedighi Moghaddam (RISE) for surface tension measurements. Cong Chen would like to thank Dr. Wenjing Sun (University of Maine) for the figure drawing assistance, Senior Scientist Seongkyung Park and Dr. Martin Yates (University of Maine) for the experimental support.

Supporting information

Formulation details and surface tension of CNC coating systems, coating performance of different formulations, POM images of casted CNC film, the optical transparency of PLA and coating films, mass change of WVTR, tear strength, and photos of water contact on CNC film.

Appendix A. Supporting information

Supplementary data associated with this article can be found in the online version at doi:10.1016/j.fpsl.2024.101244.

References

Ahankari, S. S., Subhedar, A. R., Bhadauria, S. S., & Dufresne, A. (2021). Nanocellulose in food packaging: A review. *Carbohydrate Polymers, 255*, Article 117479. https://doi.org/10.1016/j.carbpol.2020.117479

Ahmed, J., & Varshney, S. K. (2011). Polylactides—chemistry, properties and green packaging technology: a review. *International Journal of Food Properties, 14*(1), 37–58. https://doi.org/10.1080/10942910903125284

Auras, R., Harte, B., & Selke, S. (2004). An overview of polylactides as packaging materials. *Macromolecular Bioscience, 4*(9), 835–864. https://doi.org/10.1002/mabi.200400043

Auras, R. A., Harte, B., Selke, S., & Hernandez, R. (2003). Mechanical, physical, and barrier properties of poly (lactide) films. *Journal of plastic film & sheeting, 19*(2), 123–135. https://doi.org/10.1177/8756087903039702

Bhattacharya, A., & Ray, P. (2004). Studies on surface tension of poly (vinyl alcohol): effect of concentration, temperature, and addition of chaotropic agents. *Journal of Applied Polymer Science, 93*(1), 122–130. https://doi.org/10.1002/app.20436

Cazón, P., Velazquez, G., Ramírez, J. A., & Vázquez, M. (2017). Polysaccharide-based films and coatings for food packaging: A review. *Food Hydrocolloids, 68*, 136–148. https://doi.org/10.1016/j.foodhyd.2016.09.009

Chen, C., Sun, W., Wang, J., & Gardner, D. J. (2023). Tunable biocomposite films fabricated using cellulose nanocrystals and additives for food packaging. *Carbohydrate Polymers*. , Article 121315. https://doi.org/10.1016/j.carbpol.2023.121315

Chen, C., Sun, W., Wang, L., Tajvidi, M., Wang, J., & Gardner, D. J. (2022). Transparent multifunctional cellulose nanocrystal films prepared using trivalent metal ion exchange for food packaging. *ACS Sustainable Chemistry & Engineering, 10*(29), 9419–9430. https://doi.org/10.1021/acssuschemeng.2c01805

Chowdhury, R. A., Clarkson, C., Apalangya, V. A., Islam, S. M. N., & Youngblood, J. P. (2018). Roll-to-roll fabrication of cellulose nanocrystal-poly(vinyl alcohol) composite coatings with controlled anisotropy. *Cellulose, 25*(11), 6547–6560. https://doi.org/10.1007/s10570-018-2019-5

Chowdhury, R. A., Nuruddin, M., Clarkson, C., Montes, F., Howarter, J., & Youngblood, J. P. (2018). Cellulose Nanocrystal (CNC) Coatings with Controlled Anisotropy as High-Performance Gas Barrier Films. *ACS Applied Materials & interfaces, 11*(1), 1376–1383. https://doi.org/10.1021/acsami.8b16897

Coles, R., McDowell, D., & Kirwan, M. J. (2003). *Food Packaging Technology*. CRC press,.

Dhar, P., Bhardwaj, U., Kumar, A., & Katiyar, V. (2014). Cellulose nanocrystals: a potential nanofiller for food packaging applications. *Food Additives and Packaging, 1162*, 197–239. https://doi.org/10.1021/bk-2014-1162.ch017

Dhar, P., Gaur, S. S., Soundararajan, N., Gupta, A., Bhasney, S. M., Milli, M., & Katiyar, V. (2017). Reactive extrusion of polylactic acid/cellulose nanocrystal films for food packaging applications: influence of filler type on thermomechanical, rheological, and barrier properties. *Industrial & Engineering Chemistry Research, 56*(16), 4718–4735. https://doi.org/10.1021/acs.iecr.6b04699

Dhar, P., Tarafder, D., Kumar, A., & Katiyar, V. (2016). Thermally recyclable polylactic acid/cellulose nanocrystal films through reactive extrusion process. *Polymer, 87*, 268–282. https://doi.org/10.1016/j.polymer.2016.02.004

Du, L., Yu, H., Zhang, B., Tang, R., Zhang, Y., Qi, C., & Wang, J. (2021). Transparent oxygen barrier nanocellulose composite films with a sandwich structure. *Carbohydrate Polymers, 268*, Article 118206. https://doi.org/10.1016/j.carbpol.2021.118206

Fortunati, E., Peltzer, M., Armentano, I., Torre, L., Jiménez, A., & Kenny, J. (2012). Effects of modified cellulose nanocrystals on the barrier and migration properties of PLA nano-biocomposites. *Carbohydrate Polymers, 90*(2), 948–956. https://doi.org/10.1016/j.carbpol.2012.06.025

Fotie, G., Gazzotti, S., Ortenzi, M. A., & Piergiovanni, L. (2020). Implementation of high gas barrier laminated films based on cellulose nanocrystals for food flexible packaging. *Applied Sciences, 10*(9), 3201. https://doi.org/10.3390/app10093201

Gan, I., & Chow, W. (2018). Antimicrobial poly (lactic acid)/cellulose bionanocomposite for food packaging application: A review. *Food Packaging and Shelf Life, 17*, 150–161. https://doi.org/10.1016/j.fpsl.2018.06.012

Gazzotti, S., Farina, H., Lesma, G., Rampazzo, R., Piergiovanni, L., Ortenzi, M. A., & Silvani, A. (2017). Polylactide/cellulose nanocrystals: The in situ polymerization approach to improved nanocomposites. *European Polymer Journal, 94*, 173–184. https://doi.org/10.1016/j.eurpolymj.2017.07.014

Habibi, Y., Lucia, L. A., & Rojas, O. J. (2010). Cellulose nanocrystals: chemistry, self-assembly, and applications. *Chemical Reviews, 110*(6), 3479–3500. https://doi.org/10.1021/cr900339w

Haward, M. (2018). Plastic pollution of the world's seas and oceans as a contemporary challenge in ocean governance. *Nature Communications, 9*(1), Article 667. https://doi.org/10.1038/s41467-018-03104-3

Helanto, K. E., Matikainen, L., Talja, R., & Rojas, O. J. (2019). Bio-based polymers for sustainable packaging and biobarriers: a critical review. *BioResources, 14*(2), 4902–4951. https://doi.org/10.15376/biores.14.2.Helanto

Huang, S., Wang, X., Zhang, Y., Meng, Y., Hua, F., & Xia, X. (2022). Cellulose nanofibers/polyvinyl alcohol blends as an efficient coating to improve the hydrophobic and oleophobic properties of paper. *Scientific Reports, 12*(1), Article 16148. https://doi.org/10.1038/s41598-022-20499-8

Hubbe, M. A., Ferrer, A., Tyagi, P., Yin, Y., Salas, C., Pal, L., & Rojas, O. J. (2017). Nanocellulose in thin films, coatings, and plies for packaging applications: A review. *BioResources, 12*(1), 2143–2233. https://doi.org/10.15376/biores.12.1.2143-2233

Jamshidian, M., Tehrany, E. A., Imran, M., Jacquot, M., & Desobry, S. (2010). Poly-lactic acid: production, applications, nanocomposites, and release studies. *Comprehensive Reviews in Food Science and Food Safety, 9*(5), 552–571. https://doi.org/10.1111/j.1541-4337.2010.00126.x

Jariyasakoolroj, P., Leelaphiwat, P., & Harnkarnsujarit, N. (2020). Advances in research and development of bioplastic for food packaging. *Journal of the Science of Food and Agriculture, 100*(14), 5032–5045. https://doi.org/10.1002/jsfa.9497

Kargarzadeh, H., Mariano, M., Huang, J., Lin, N., Ahmad, I., Dufresne, A., & Thomas, S. (2017). Recent developments on nanocellulose reinforced polymer nanocomposites: A review. *Polymer, 132*, 368–393. https://doi.org/10.1016/j.polymer.2017.09.043

Karkhanis, S. S., Stark, N. M., Sabo, R. C., & Matuana, L. M. (2018). Water vapor and oxygen barrier properties of extrusion-blown poly (lactic acid)/cellulose nanocrystals nanocomposite films. *Composites Part A: Applied Science and Manufacturing, 114*, 204–211. https://doi.org/10.1016/j.compositesa.2018.08.025

Kawashima, N., Yagi, T., & Kojima, K. (2019). How do bioplastics and fossil-based plastics play in a circular economy? *Macromolecular Materials and Engineering*. https://doi.org/10.1002/mame.201900383

Le Gars, M., Dhuiège, B., Delvart, A., Belgacem, M. N., Missoum, K., & Bras, J. (2020). High-barrier and antioxidant poly (lactic acid)/nanocellulose multilayered materials for packaging. *ACS Omega*. https://doi.org/10.1021/acsomega.0c01955

Liu, Y., & Matuana, L. M. (2019). Surface texture and barrier performance of poly (lactic acid)–cellulose nanocrystal extruded-cast films. *Journal of Applied Polymer Science, 136*(22), Article 47594. https://doi.org/10.1002/app.47594

Marsh, K., & Bugusu, B. (2007). Food packaging—roles, materials, and environmental issues. *Journal of Food Science, 72*(3), R39–R55. https://doi.org/10.1111/j.1750-3841.2007.00301.x

Moll, C. J., Meister, K., Kirschner, J., & Bakker, H. J. (2018). Surface Structure of Solutions of Poly (vinyl alcohol) in Water. *The Journal of Physical Chemistry B, 122* (47), 10722–10727. https://doi.org/10.1021/acs.jpcb.8b08374

Mu, R., Hong, X., Ni, Y., Li, Y., Pang, J., Wang, Q., & Zheng, Y. (2019). Recent trends and applications of cellulose nanocrystals in food industry. *Trends in Food Science & Technology, 93*, 136–144. https://doi.org/10.1016/j.tifs.2019.09.013

Muller, J., González-Martínez, C., & Chiralt, A. (2017). Combination of poly (lactic) acid and starch for biodegradable food packaging. *Materials, 10*(8), 952. https://doi.org/10.3390/ma10080952

Narancic, T., & O'Connor, K. E. (2018). Plastic waste as a global challenge: are biodegradable plastics the answer to the plastic waste problem? *Microbiology, 165* (2), 129–137. https://doi.org/10.1099/mic.0.000749

Nuruddin, M., Chowdhury, R. A., Szeto, R., Howarter, J. A., Erk, K. A., Szczepanski, C. R., & Youngblood, J. P. (2021). Structure–Property Relationship of Cellulose Nanocrystal–Polyvinyl Alcohol Thin Films for High Barrier Coating Applications. *ACS Applied Materials & interfaces, 13*(10), 12472–12482. https://doi.org/10.1021/acsami.0c21525

Peng, B., Tang, J., Wang, P., Luo, J., Xiao, P., Lin, Y., & Tam, K. C. (2018). Rheological properties of cellulose nanocrystal-polymeric systems. *Cellulose, 25*, 3229–3240. https://doi.org/10.1007/s10570-018-1775-6

Piergiovanni, L., & Limbo, S. (2016). *Food Packaging Materials*. Springer,. https://doi.org/10.1007/978-3-319-24732-8

Qasim, U., Osman, A. I., Al-Muhtaseb, A. a H., Farrell, C., Al-Abri, M., Ali, M., & Rooney, D. W. (2021). Renewable cellulosic nanocomposites for food packaging to avoid fossil fuel plastic pollution: a review. *Environmental Chemistry Letters, 19*(1), 613–641. https://doi.org/10.1007/s10311-020-01090-x

Reddy, M. M., Vivekanandhan, S., Misra, M., Bhatia, S. K., & Mohanty, A. K. (2013). Biobased plastics and bionanocomposites: Current status and future opportunities. *Progress in Polymer Science, 38*(10-11), 1653–1689. https://doi.org/10.1016/j.progpolymsci.2013.05.006

Rošic, R., Pelipenko, J., Kristl, J., Kocbek, P., Bešter-Rogač, M., & Baumgartner, S. (2013). Physical characteristics of poly (vinyl alcohol) solutions in relation to electrospun nanofiber formation. *European Polymer Journal, 49*(2), 290–298. https://doi.org/10.1016/j.eurpolymj.2012.11.013

Sangroniz, A., Zhu, J.-B., Tang, X., Etxeberria, A., Chen, E. Y.-X., & Sardon, H. (2019). Packaging materials with desired mechanical and barrier properties and full chemical recyclability. *Nature Communications, 10*(1), 1–7. https://doi.org/10.1038/s41467-019-11525-x

Stark, N. M. (2016). Opportunities for cellulose nanomaterials in packaging films: A review and future trends. *Journal of Renewable Materials, 4*(5), 313–326. https://doi.org/10.7569/JRM.2016.634115

Sung, S. H., Chang, Y., & Han, J. (2017). Development of polylactic acid nanocomposite films reinforced with cellulose nanocrystals derived from coffee silverskin. *Carbohydrate Polymers, 169*, 495–503. https://doi.org/10.1016/j.carbpol.2017.04.037

Takkalkar, P., Tobin, M. J., Vongsvivut, J., Mukherjee, T., Nizamuddin, S., Griffin, G., & Kao, N. (2019). Structural, thermal, rheological and optical properties of poly (lactic acid) films prepared through solvent casting and melt processing techniques. *Journal of the Taiwan Institute of Chemical Engineers, 104*, 293–300. https://doi.org/10.1016/j.jtice.2019.08.018

Trache, D., Hussin, M. H., Haafiz, M. K., & Thakur, V. K. (2017). Recent progress in cellulose nanocrystals: sources and production. *Nanoscale, 9*(5), 1763–1786. https://doi.org/10.1039/c6nr09494e

Ureña-Benavides, E. E., Ao, G., Davis, V. A., & Kitchens, C. L. (2011). Rheology and phase behavior of lyotropic cellulose nanocrystal suspensions. *Macromolecules, 44*(22), 8990–8998. https://doi.org/10.1021/ma201649f

Wang, J., Gardner, D. J., Stark, N. M., Bousfield, D. W., Tajvidi, M., & Cai, Z. (2018). Moisture and Oxygen Barrier Properties of Cellulose Nanomaterial-Based Films. *ACS Sustainable Chemistry & Engineering, 6*(1), 49–70. https://doi.org/10.1021/acssuschemeng.7b03523

Wang, L., Chen, C., Wang, J., Gardner, D. J., & Tajvidi, M. (2020). Cellulose nanofibrils versus cellulose nanocrystals: Comparison of performance in flexible multilayer films for packaging applications. *Food Packaging and Shelf Life, 23*, Article 100464. https://doi.org/10.1016/j.fpsl.2020.100464

Wang, L., Gardner, D. J., Wang, J., Yang, Y., Tekinalp, H. L., Tajvidi, M., & Han, Y. (2020). Towards industrial-scale production of cellulose nanocomposites using melt processing: a critical review on structure-processing-property relationships. *Composites Part B: Engineering, 201*, Article 108297. https://doi.org/10.1016/j.compositesb.2020.108297

Wu, N., Dai, J., & Micale, F. J. (1999). Dynamic surface tension measurement with a dynamic Wilhelmy plate technique. *Journal of Colloid and Interface Science, 215*(2), 258–269.

Xu, Y., Atrens, A. D., & Stokes, J. R. (2017). Rheology and microstructure of aqueous suspensions of nanocrystalline cellulose rods. *Journal of Colloid and Interface Science, 496*, 130–140. https://doi.org/10.1016/j.jcis.2017.02.020

Youngblood, J.P., Azrak, S.M.E.A., Moon, R.J., & Schueneman, G.T. (2022). Composition of cellulose nanocrystals and carboxymethyl cellulose. Google Patents.